





Article

Role of the Biogenic Carbon Physicochemical Properties in the Manufacturing and Industrial Transferability of Mill Scale-Based Self-Reducing Briquettes

Gianluca Dall'Osto , Davide Mombelli * , Sara Scolari  and Carlo Mapelli 

Dipartimento di Meccanica, Politecnico di Milano, Via La Masa 1, 20156 Milano, Italy; gianluca.dallosto@polimi.it (G.D.); sara.scolari@polimi.it (S.S.); carlo.mapelli@polimi.it (C.M.)

* Correspondence: davide.mombelli@polimi.it

Abstract: The recovery of iron contained in mill scale rather than iron ore can be considered a promising valorization pathway for this waste, especially if carried out through reduction using biogenic carbon sources. Nevertheless, the physicochemical properties of the latter may hinder the industrial transferability of such a pathway. In this work, the mechanical and metallurgical behavior of self-reduced briquettes composed of mill scale and four biogenic carbons (with increasing ratios of fixed carbon to volatile matter and ash) was studied. Each sample achieved mechanical performance above the benchmarks established for their application in metallurgical furnaces, although the presence of alkali compounds in the ash negatively affected the water resistance of the briquettes. In terms of metallurgical performance, although agglomeration successfully exploited the reduction by volatiles from 750 °C, full iron recovery and slag separation required an amount of fixed carbon higher than 6.93% and a heat treatment temperature of 1400 °C. Finally, the presence of Ca-, Al-, and Si- compounds in the ash was essential for the creation of a slag compatible with steelmaking processes and capable of retaining both phosphorus and sulfur, hence protecting the recovered iron.

Keywords: agglomeration; biogenic carbon; carbothermic reduction; iron recovery; mill scale; physicochemical properties; waste valorization



Citation: Dall'Osto, G.; Mombelli, D.; Scolari, S.; Mapelli, C. Role of the Biogenic Carbon Physicochemical Properties in the Manufacturing and Industrial Transferability of Mill Scale-Based Self-Reducing Briquettes. *Metals* **2024**, *14*, 882. <https://doi.org/10.3390/met14080882>

Academic Editor: Corby G. Anderson

Received: 8 July 2024

Revised: 29 July 2024

Accepted: 29 July 2024

Published: 30 July 2024



Copyright: © 2024 by the authors. Licensee MDPI, Basel, Switzerland. This article is an open access article distributed under the terms and conditions of the Creative Commons Attribution (CC BY) license (<https://creativecommons.org/licenses/by/4.0/>).

1. Introduction

Among the main industrial sectors, steelmaking is considered a pillar of societal development on a global scale, with its proliferation intimately linked to a growing and successful economy [1]. At present, steel is the most produced and consumed material for engineering applications, with a crude steel production of more than 1850 Mton in 2023 [2]. Nonetheless, the amount of CO₂ emissions from the steel production processes (5% and 7% of European and global human emissions, respectively) makes it a hard-to-abate sector with an urgent need to develop new low-carbon technologies and find new sources of materials that can make it independent from both mineral extraction from natural reserves and fossil carbon exploitation [3]. As a consequence, all major steel producers are currently following what could be called the transition from the primary steelmaking era, based on the use of sintering plant (SP), blast furnace (BF), and basic oxygen furnace (BOF) plants, to the electric steelmaking era, which consists of recycling scrap in electric arc furnaces (EAF) or electric melting furnaces (ESF), possibly coupled with direct reduction plants (DRP) [3]. Although this transition appears to be a possible solution to align with the EU climate goals, it will also result in increased demand for high-quality scrap and iron ore, the latter of which is needed for the production of direct reduced iron (DRI) or hot briquetted iron (HBI) to dilute the amount of harmful elements brought into the bath if low-grade scrap (i.e., scrap subject to two or three remelts over time) are used [4].

In this regard, the utilization of steel mill wastes and by-products rather than ores to produce clean iron could be a viable and cost-effective strategy to avoid mining. In fact, at

a closer look, the steel industry has a wide range of iron oxide-bearing residues that have not yet been fully exploited, leaving several small material loops waiting to be closed [5]. Among various wastes and residues, mill scale (MS) is one of the most significant examples, as it consists of more than 90 wt.% iron oxides and is closely linked to the steel production, being generated during the hot working of steel and iron products and accounting for 2 wt.% of the steel produced. Depending on grain size and oil content, MS is used as feed in SP [6], sold cheaply to other sectors (e.g., construction [7], refractory [8], pigment [9]) or, in the worst case, disposed of in landfills, resulting in the loss of a source of clean iron and the need for economic expenditures for steel production. However, according to Iluțiu-Varvara et al. [10], it is estimated that approximately more than 30% of MS is still not fully valorized worldwide.

The first attempts of MS valorization date back to the mid-1960s, when Khodakovskii et al. [11] and Manukyan et al. [12] investigated the feasibility of its exploitation as a starting material to produce pure iron powder and sponge. Although this line of research has continued and expanded to the present day with studies based on carbothermal [13–15], aluminothermic [16–18], and gas-based (e.g., CO and H₂) reduction processes [19–21], the findings were not easily transferable to an industrial scale. The main reasons were due to the use of fossil carbon sources, unsuitable process parameters (e.g., temperature or time), economically expensive reducing elements (e.g., Al), or non-acceptable chemical and granulometric properties of the reduced iron particle for the introduction to the furnaces.

According to the BREF Best Available Techniques (BAT) Reference Document for Iron and Steel production [6], although most MS finds its main route of use/valorization in SP (along with dusts and sludges), the relative percentage in feed commonly stops at about 5–6% and only in rare cases reaches 10–20%. The main limitations are due to the negative impact that some elements (e.g., Zn, Pb, and chlorides) would have on the subsequent reintroduction of the sintered product into the BF. It is worth noting that the use of oily MS as feedstock in SP has also been studied, but even in these studies, the main difficulties were found to be the volatilization of hydrocarbon impurities (0.3–10 wt.%), which clogged the filter bags resulting in a fire hazard, increased dust production, and an overall decrease in productivity [22,23].

This was due to the significant amounts of particles smaller than 200 μm in MS, which nevertheless make it very attractive and suitable for the creation of agglomerates (e.g., briquettes or pellets) rather than its direct injection into furnaces [10].

As a parallel decarbonization route, the research on the total or partial replacement of fossil carbon sources with biogenic sources (e.g., biochar, biocoke, or hydrochar, generally labeled from now on as BC) has been highly active in recent years, due to the carbon neutrality associated with such kinds of materials. Several trials have been performed both in the primary and electric steelmaking routes on the actual feasibility of their exploitation as a coal substitute [24–27], carburizing agent [27,28], and foaming agent [29,30]. However, the inherent heterogeneity of the biochar physicochemical properties and general chemistry, resulting from both the starting biomass (e.g., woody matrix, food waste, sludge) and the production process (e.g., pyrolysis, torrefaction, hydrothermal carbonization), provided erratic results. On the one hand, satisfactory results were achieved when the properties were comparable to those of coke and coal; on the other hand, the early and strong gasification of low fixed carbon biochars inhibited their effectiveness and in some cases led to overheating and the subsequent shutdown of the dedusting system [31,32]. Nevertheless, the gasification of the low-grade BC could be beneficial because volatile evolution can contribute, to some extent, to the reduction of higher iron oxidation states (hematite and magnetite) at temperatures below 800 °C [33–35]. Despite the significant potential and environmental benefits of applying BC sources as reducing agents for iron recovery through the carbothermal reaction, there is currently a significant disproportion of studies exploiting iron ores as oxide-bearing materials [36–42] rather than MS [43–45].

Following the paradigms of waste utilization for mineral resource conservation and fossil carbon independence, this work focuses on the mechanical and metallurgical charac-

terization of MS/BC self-reducing briquettes, with specific attention being paid to the effect of the physicochemical properties of the biogenic carbon source on the reduction behavior. The main challenges addressed are the achievement of the required characteristics for the introduction of such briquettes into the main steelmaking furnaces (e.g., BF, EAF, ESF, cupola furnaces, fluidized bed reactors, and rotary hearth furnaces), as well as the effective recovery of iron even when using low-grade BC. For this purpose, MS was mixed with four BC matrices, and, maintaining the low environmental impact of the process, an organic binder (corn starch) was exploited as a binding agent. Finally, although this study focuses on understanding the behavior of low- to high-grade MS/BS agglomerates, the results are also relevant to the establishment and the strengthening of the industrial symbiosis of the steel sector with major biomass-producing sectors (e.g., wooden/furniture, agricultural, and wastewater treatment plants).

2. Materials and Methods

2.1. Materials and Characterization

The briquettes were produced through agglomeration of the iron oxide-bearing matrix, rolling mill scale (MS), and four biogenic carbon matrices with increasing volatile matter content used as reducing agents and related to the wood, agriculture, and wastewater treatment sectors, namely, commercial wood pellets pyrolyzed at 750 °C for 25 min (WC), agricultural-derived olive pomace pyrolyzed at 750 °C and 350 °C for 25 min (OP750 and OP350), and sewage sludge hydrothermally carbonized at 210 °C at 20 bar (HC).

Prior to agglomeration, the MS was characterized by wavelength-dispersive X-ray fluorescence (WD-XRF) and X-ray diffraction (XRD) analysis to evaluate the chemical composition and mineralogical composition, the latter quantified by Rietveld method. The summary of the results is given in Table 1, and the XRD pattern is shown in the supplementary material (Figure S1).

Table 1. Chemical and mineralogical composition of mill scale (wt.%).

Wavelength-Dispersive X-ray Fluorescence								Rietveld Analysis			
Al ₂ O ₃	CaO	Cr ₂ O ₃	CuO	Fe ₂ O ₃	MgO	MnO	NiO	SiO ₂	Wustite	Magnetite	Hematite
0.30	0.32	0.45	0.10	96.95	0.07	1.13	0.08	0.60	60	30	10

The four reducing agents were characterized before agglomeration in terms of (i) percentage of fixed carbon, volatile, and ash by proximate analysis [46,47]; (ii) amount of total carbon and sulfur content by LECO analysis; (iii) activation energy by Kissinger–Akahira–Sunose (KAS) method [48]; (iv) water contact angle by sessile drop method [49]; and (v) mineralogical composition by XRD analysis. The summary of the physicochemical properties is given in Table 2; the XRD patterns of the reducing agents are given in the supplementary material (Figure S2).

Table 2. Proximate analysis, total carbon and sulfur content, activation energy, and water contact angle of reducing agents (WC: wood pellets pyrolyzed at 750 °C, OP750: olive pomace pyrolyzed at 750 °C, OP350 olive pomace pyrolyzed at 350 °C, HC: sewage sludge hydrothermally carbonized at 210 °C, C_{fix}: fixed carbon, VM: volatile matter, C_{tot}: total carbon, S: sulfur, E_a: activation energy, db: dry basis).

	Proximate Analysis (wt.% _{db})			C _{tot} (wt.%)	S (wt.%)	Activation Energy (kJ mol ⁻¹)	Contact Angle (deg.)
	C _{fix}	VM	Ash				
WC	83.81	12.58	3.61	93.51	0.001	110.45	71.75
OP750	31.14	51.9	16.96	69.87	0.109	86.76	52.02
OP350	21.22	62.55	16.22	65.23	0.059	74.52	146.98
HC	0.73	69.95	29.32	42.67	0.589	61.61	157.84

2.2. Powder Briquetting

The materials were ground separately in a planetary ball mill with zirconium balls; subsequently, the mill scale was sieved to very fine sand (63–125 μm) and the reducing agents to coarse silt (less than 63 μm) to maximize the packing factor and reaction kinetics [50,51].

Four different recipes were obtained by adjusting the amount of reducing agent introduced to the stoichiometric carbon required for the reduction of all iron oxide contained in the mill scale ($C_{\text{tot}}/\text{FeO}_{\text{eq}}$ equal to 0.2). The amount of MS in the recipe and that of fixed carbon, volatile matter, and ash (contributed by the reducing agent) are given in Table 3.

Table 3. Recipe composition (MS: mill scale, WC: wood pellets pyrolyzed at 750 °C, OP750: olive pomace pyrolyzed at 750 °C, OP350 olive pomace pyrolyzed at 350 °C, HC: sewage sludge hydrothermally carbonized at 210 °C, C_{fix} : fixed carbon, VM: volatile matter, db: dry basis).

	Mill Scale	C_{fix}	VM	Ash
	(wt.% _{db})			
MS/WC	82.38	14.77	2.22	0.64
MS/OP750	77.75	6.93	11.55	3.77
MS/OP350	76.53	4.98	14.68	3.81
MS/HC	68.08	0.23	22.32	9.36

Corn starch was used as organic binder and dosed to correspond to 5 wt.% of the dry MS/BC pre-mix. To obtain a binder with a retrogradation rate of 30%, considered as the percentage able to provide the best mechanical performance to the agglomerates, distilled water (starch/water ratio of 1:6 by weight) was added to the starch and heated at 80 °C for 50 min [51]. The binder was immediately added to the recipe and then pressed with a constant speed of 20 mm min⁻¹ until 40 MPa and maintained for 2 min, using a modified MTS Exceed Series 40 (MTS Systems, Eden Prairie, MN, USA) uniaxial tensile test machine (specific details of the machine are given in an earlier study by the authors [52]).

Cylindric briquettes of 20 mm in diameter, 20 mm in height, and about 15 g in mass were produced and dried for 14 days, during which the mass and volume of each briquette was monitored to evaluate the green and cured apparent density. To obtain a clear estimation of the volume, the samples were digitally processed into 3D spatial data by means of Agisoft Metashape photogrammetric processing software (version 1.8.5, Agisoft LLC, St. Petersburg, Russia).

2.3. Mechanical Characterization

The briquettes were mechanically characterized through impact resistance, cold compression, and water immersion resistance tests. Three replications were performed for each test to verify the reproducibility of the results.

Impact resistance was used to simulate falling briquettes inside a furnace; the ASTM D440-07 (2019) [53] was used as a guideline. Samples were dropped from a height of 1.63 m inside a tube with a vessel and stopped in case the briquettes withstood up to 10 falls or in case of premature failure. The impact resistance index (IRI) was calculated according to (1) whereas the detached material after each fall was collected, sieved, and weighed to estimate the size stability factor (s) according to (2).

$$\text{IRI} = \frac{n}{N} \times 100 \quad (1)$$

$$s(\%) = \sum_i wt_i \cdot \frac{\text{Sieve Opening}_i}{\text{Biggest Sieve Opening}} \times 100 \quad (2)$$

where n is the number of drops prior to failure, N is the number of pieces detached weighing 5% or more of the starting mass, and wt_i is the mass fraction of powder with respect to the

starting mass retained in the *ith* sieve; specifically, the apertures used were 6.7 mm, 5.6 mm, 4 mm, 2 mm, 1 mm, 0.5 mm, and 0.125 mm.

Cold compression test was used to simulate the stresses at which the briquettes are subjected during the transportation or inside the furnace, the BS ISO 4700:2015 standard was used as a guideline [54]. The sample was pre-loaded between 2 flat plates at 30 N and pressed at a constant speed of 15 mm min⁻¹ until the load falls by 50% of the ultimate compressive strength (UCS), or when the gap between the plates was reduced by more than 50% of the briquette diameter (10 mm).

The water resistance test was used to simulate the behavior of briquettes when exposed to rain or high humidity conditions that may adversely affect the quality of the densified product; the procedure described by Richards [55] was used as a guideline. The sample was fully immersed in distilled water at room temperature, removed after 600, 1200, and 1800 s, cleaned of surface moisture, and weighed each time. In addition, the visual appearance of the samples was constantly monitored by camera. The water resistance index (WRI) was calculated at 1800 s according to (3).

$$\text{WRI}(\%) = \left(1 - \frac{w_{1800\text{s}} - w_0}{w_0} \right) \times 100 \quad (3)$$

where $w_{1800\text{s}}$ and w_0 are the mass of the sample after 1800 s and the initial one, respectively.

2.4. Metallurgical Performances Characterization

2.4.1. Reduction Behavior

The samples were thermally treated at four temperatures (750, 900, 1050 and 1200 °C) under inert atmosphere to evaluate the swelling, mineralogical evolution mass loss and degree of reduction subsequent to the heating.

The thermal cycles were carried in a Nabertherm LHT 02/17 LB lift-bottom furnace (Nabertherm, Lilienthal, Germany) in which a crucible containing the sample was inserted. The crucible was made in alumina and, to prevent any interaction with the briquette, a second graphite crucible was used as sample container. Since no variation of mass was observed in the graphite crucible in the experimental trials, it was concluded that it did not affect the results. To ensure an inert atmosphere, an argon flow (10·NI h⁻¹) was directly blown inside the alumina crucible during the whole treatment duration. Specifically, after a first maintenance at room temperature of 30 min, required to saturate the crucible volume with argon, the target temperature was reached using a heating rate of 100 °C min⁻¹ and maintained for 15 min; finally, the crucible was naturally cooled down in the oven and extracted below 300 °C. The crucible configuration is given in Figure 1.

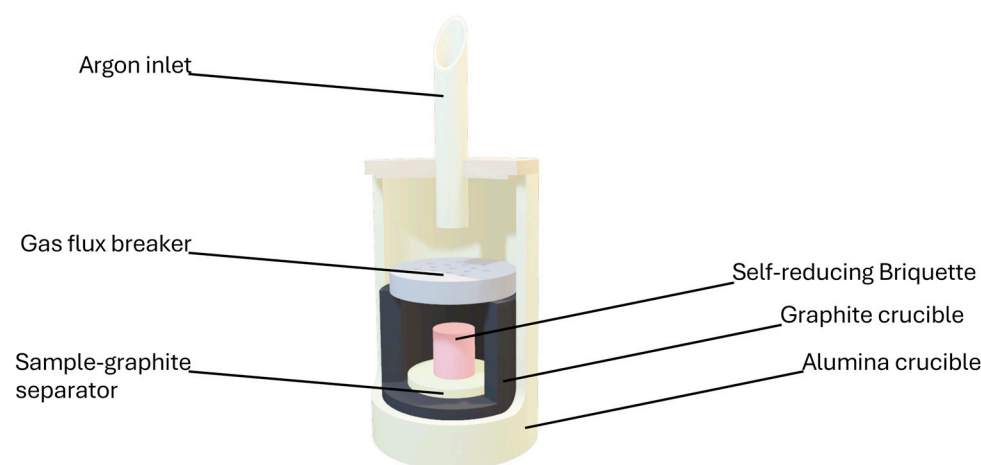


Figure 1. Schematics of the crucible used for the thermal treatment testing.

The swelling index was evaluated considering the apparent volume of the briquettes assuming the absence of internal porosities and according to (4).

$$\text{Swelling (\%)} = \frac{V_i - V_0}{V_0} \times 100 \quad (4)$$

where V_i and V_0 are the sample volume after the thermal cycle and the initial one, respectively. To obtain a clear estimation of the volume, the samples were digitally processed into 3D spatial data by means of Agisoft Metashape photogrammetric processing software (version 1.8.5, Agisoft LLC, St. Petersburg, Russia).

To focus on the role of the physicochemical properties of the reducing agents alone, the mass loss of the briquettes was evaluated by excluding the mass of the binder, assuming that it does not contribute largely to the reduction of iron oxides and calculated according to (5).

$$\Delta m (\%) = \frac{w_i - w_0}{w_0} \times 100 \quad (5)$$

where w_i and w_0 are the sample mass after the thermal cycle and the initial one, respectively (both masses were evaluated considering only the iron-bearing matrix and the reducing agent).

As pointed out by Vitikka et al. [43], carbon gasification during heating is responsible for the degree of reduction (DoR) bias in the case of self-reducing agglomerates with biogenic carbon sources. Consequently, to overcome this shortcoming, a modified version of BS ISO 11258:2015 [56], reported in (6), was used in this study to also take it into account.

$$\text{DoR (\%)} = \frac{w_i - w_0}{w_{th} - w_0} \times 100 \quad (6)$$

where w_{th} is the theoretical mass loss, calculated as the sum of the total expected losses from CO evolution (related to the reduction of oxides) and that of the removal of non-carbon volatile matter (related to the gasification during heating). Specifically, the former was evaluated by considering the complete conversion of C_{tot} present in the sample into CO, while the latter from the proximate analysis results as the difference between volatile matter and that of C_{tot} and C_{fix} ($VM - (C_{tot} - C_{fix})$).

Mineralogical evolution was determined by XRD analysis using a Rigaku Smartlab SE diffractometer (Rigaku Corporation, Tokyo, Japan) with $\text{CuK}\alpha$ radiation ($\lambda = 1.54 \text{ \AA}$) equipped with XRF suppression 1D detector (D/Tex 250). The samples were scanned from 20 to $120^\circ 2\theta$ at 1° min^{-1} with a step size of 0.02° and rotated at 120 rpm to decrease texture contribution.

2.4.2. Smelting Behavior and Iron Recovery

A fifth thermal treatment at 1400°C , still under inert atmosphere, was conducted to investigate the feasibility of achieving the smelting of the reduced iron and its microstructure. In cases in which the briquette maintained its agglomerate morphology, the samples were cut in half to expose the cross section, mounted using a phenolic resin, and polished up to $1 \mu\text{m}$. Otherwise, the reduced iron droplets were directly mounted and polished.

Metallographic analysis was carried out through optical microscopy whereas a Zeiss Sigma 300 Field Emission Gun Electronic Scanning Microscope (FEG-SEM) equipped with an Oxford Xmax Ultim 65 Energy-Dispersive X-ray Spectroscopy (EDS) probe (Carl Zeiss AG, Jena, Germany) was exploited to map the phase distribution at the end of the reduction process.

Finally, the degree of metallization (DoM) at 1400°C was determined by quantitative metallurgy [57] by the post-processing of five backscatter electron micrographs taken stochastically along the polished surface of the sample and calculated according to (7).

$$\text{DoM (\%)} = \frac{Fe_M}{Fe_T} \times 100 = \frac{n_{Fe} \cdot \rho_{Fe}}{n_{Fe} \cdot \rho_{Fe} + n_{FeO} \cdot \rho_{FeO} \cdot \chi} \times 100 \quad (7)$$

where Fe_M is the metallic iron, Fe_T is the total iron, n_{Fe} is the number of pixels attributed to the metallic iron, ρ_{Fe} is the metallic iron density, n_{FeO} is the number of pixels attributed to the oxide iron, ρ_{FeO} is the oxide iron density, and χ is the weight percentage of iron in the specific oxide observed.

3. Results

3.1. Briquette Mechanical Performances

The as-produced briquettes (green) were let dry at room temperature to allow their curing and density stabilization. The visual appearance of the briquettes after 14 days (cured) is shown in Figure 2.

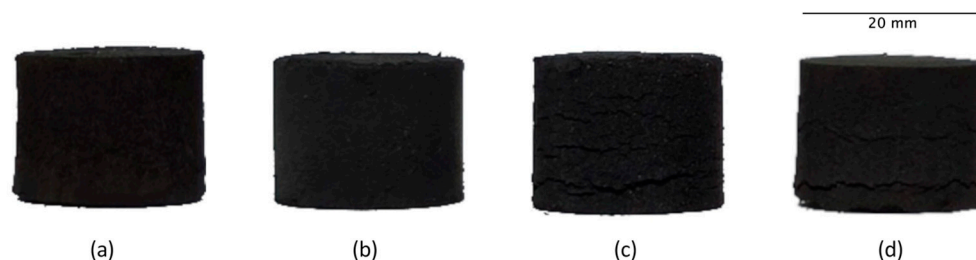


Figure 2. Appearance of the briquettes after 14 days of curing (a) MS/WC, (b) MS/OP750, (c) MS/OP350, and (d) MS/HC.

Although each briquette was able to self-sustain after the curing period, the surface of MS/WC and MS/OP750 samples differed strongly from that of MS/OP350 and MS/HC. On the one hand, the first two recipes were able to produce an agglomerate with a compact and smooth surface, while on the other hand, the MS/OP350 and MS/HC briquettes were characterized by the presence of several longitudinal cracks. Their presence is synonymous of a poor powder compaction, which makes the agglomerate unable to accommodate the shear stresses generated during the demolding step [58]. The differences in compaction behavior may also be associated with the presence of graphitic and amorphous carbon in WC and OP750 (Figure S2a,b), which acted as a lubricant during both the compression and demolding stages, reducing friction against the mold walls and the related shear stresses, in contrast to cellulose or hemicellulose in OP350 and HC (Figure S2c,d). Furthermore, it is worth noting that during the curing period, the hydrophobic nature of OP350 and HC (Table 2) may have favored the removal of moisture from the binder resulting in a widening of the cracks themselves. The apparent density of the briquettes and their mechanical properties are given in Table 4.

Table 4. Apparent density and mechanical properties of the briquettes (standard deviation in parenthesis).

	MS/WC	MS/OP750	MS/OP350	MS/HC
Apparent density, green (g cm^{-3})	2.48 (0.06)	2.69 (0.04)	2.33 (0.06)	2.35 (0.06)
Apparent density, cured (g cm^{-3})	2.34 (0.04)	2.57 (0.05)	2.16 (0.05)	2.24 (0.07)
Number of drop/1.63 m	10.0 (0.0)	9.5 (0.5)	3.0 (2.0)	7.7 (1.2)
Impact resistance index	1000.0 (0.0)	766.7 (230.2)	75.0 (22.5)	230.0 (4.8)
Size stability (%)	99.60 (3.64)	96.02 (1.63)	76.01 (10.52)	86.33 (6.11)
Ultimate compressive strength (MPa)	15.39 (0.19)	12.56 (0.74)	3.91 (0.56)	6.33 (0.74)
Water resistance index (%)	90.41	Failed before 600 s	Failed before 600 s	80.45

Each agglomerate underwent a decrease in apparent density from a green to cured state due to starch retrogradation, reaching a final value between 2.16 and 2.57 g cm^{-3} [51]. Although these values do not pose significant problems in their handling, transport, and storage, the slightly lower apparent densities, compared with that of EAF slag (2.98 g cm^{-3} at 1873 K), would result in their floating on the melt, with a consequent loss in iron

recovery capacity if introduced directly into the furnace [59]. One possible solution is their placement in the lower layers of the charge to allow reduction during the first heating phase and the parallel increase in density due to the conversion of iron oxide to metallic iron. Conversely, since in the BF, cupola, and rotary heart processes the charge is solid, this problem would be less impactful as well as in line with the quality reference values of iron oxide pellets used in the aforementioned furnaces ($2\text{--}2.5\text{ g cm}^{-3}$) [60].

The difference in the specific apparent density, both in the green and cured states, is mainly related to three recipe-specific properties: (1) the relative mass ratio between MS and the reducing agent—the greater the value the greater the density, (2) the volumetric particle size distribution—the smaller the overall particle size the lower the density, and (3) the amount of inorganic content (ash) in the reducing agent—the greater the ash the higher the density [61]. The consequences of the specific recipe characteristics on the apparent density are most appreciable in the MS/WC and MS/OP750 briquettes comparison due to their compactness. Indeed, although the former was characterized by a greater amount of MS and a consequent particle size more oriented toward $125\text{ }\mu\text{m}$, the greater amount of inorganic matter present in the latter was responsible for the higher density observed [62]. In addition, the lower hydrophilicity of WC enhanced the removal of moisture from the briquette during the curing period, leading to a greater decrease in density in the MS/WC briquette than in MS/OP750 (5.64% vs. 4.46%) [51]. The presence of cracks in the MS/OP350 and MS/HC briquettes distorted the apparent density measurements in the cured state, decreasing its value. Nevertheless, considering only the green state of the MS/OP350 and MS/HC briquettes, they were characterized by the lowest apparent densities among the samples, confirming the role of the relative mass ratio between the recipe powders and the volumetric particle size distribution discussed by Zhang et al. [61]. Finally, it is interesting to note that the direct comparison of the MS/OP350 and MS/HC cured briquettes showed a higher apparent density of the latter due to the higher amount of ash in the starting recipe.

The number of drops from a standstill to failure was, in ascending order of performance, 1 to 5 times/1.63 m for MS/OP350, 7 to 9 times/1.63 m for MS/HC, 9 to 10 times/1.63 m for MS/OP750, and 10 times/1.63 m for MS/WC. In addition, because this latter managed to remain intact until the tenth fall, its IRI resulted equal to 1000, while, despite the similar impact resistance of the MS/OP750 briquette, its IRI was found to be 766.7, due to its breakage during the last falls. The excellent impact resistance of the MS/WC and MS/OP750 samples is also reflected in their respective size stability of 99.60 and 96.02%, which means the low dispersion of fines after impact. Although the MS/HC and MS/OP350 briquettes showed the lowest IRI, namely 230 and 75, the values were still above the benchmark for handling and transporting briquettes for industrial applications ($\text{IRI} > 50$), with acceptable dispersion of fines after their failure ($s > 75\%$) due to the binding effect given by corn starch, and with a number of drops before failure equal to or greater than that required by the iron oxide agglomerates used in BFs or shaft furnaces (drops before failure > 4) [60,63].

The difference in impact resistance between the MS/WC and MS/OP750 briquettes and the MS/OP350 and MS/HC briquettes is indirectly attributable to the physicochemical properties of the reducing agents. Indeed, due to the lower compactability of OP350 and HC with MS, the cracks and fissures on the final surface of the briquettes, as well as the possible presence of porosity within the matrix of the briquettes themselves, acted as sources of stress and points of failure during impact [61,64].

The compression results followed the identical order of impact strength performance: the highest UCS was observed for the MS/WC briquette (15.39 MPa), followed closely by the MS/OP750 one (12.56 MPa), while the MS/HC briquette (6.33 MPa) performed intermediately between the first two samples and the MS/OP350 briquette (3.91 MPa). Regardless, each briquette exceeded the reference value required for industrial storage and loading on conveyor belts (0.375 MPa) as well as that required for iron oxide agglomerates used in BFs or shaft furnaces ($\text{UCS} > 7.9\text{--}9.5\text{ MPa}$) [60,63].

The higher compressive strength of the MS/WC and MS/OP750 briquettes is consistent with the observations of El-Hussiny and Shalabi [65], who observed an increase in the UCS of briquettes proportional to the amount of MS present, at a constant amount of binder and agglomeration pressure.

Only the MS/WC and MS/HC briquettes were able to withstand immersion in water up to 1800 s, with a water absorption of 9.59 and 19.55%, respectively. According to Davies and Davies [66], the water resistance is inversely proportional to the amount of porosity of the briquette, which explained the lower water absorption of MS/WC briquette compared with the MS/HC briquette, despite the hydrophilic nature of WC compared with the hydrophobic of HC. On the one hand, the smooth surface of the MS/WC briquette prevented the infiltration of water, limiting the mass gain to the hydration of the superficial WC particles. On the other, the presence of cracks in the MS/HC briquette allowed the infiltration of water into the porosity, as suggested by the expulsion of bubbles from the briquette during the immersion (Figure S3a,d).

In contrast, both briquettes produced with OP as the reducing agent disintegrated rapidly upon contact with water (before 600 s of immersion), suggesting the presence of collateral properties of the reducing agents that affect water resistance. The main difference between the OP750 and OP350 reducing agents compared with WC and HC lies in the presence of water-soluble sylvite (KCl) (Figure S2b,c), which act as a catalyst for the dissolution of calcite (CaCO_3) when in contact with water [67]. Specifically, the dissolution of calcite increased the number of porosities present, exposing more of the hydrophilic OP750 particles to hydration, hence causing the briquette to swell severely to the point of failure (Figure S3b). Conversely, the hydrophobic nature of OP350 inhibited the particles' hydration and related swelling, confining the failure mechanisms to the loss of mechanical continuity due to the dissolution of sylvite and calcite (Figure S3c).

3.2. Metallurgical Performance Characterization

Figure 3 shows the mineralogical evolution of the briquettes after heating at 750, 900, 1050, and 1200 °C under Ar atmosphere.

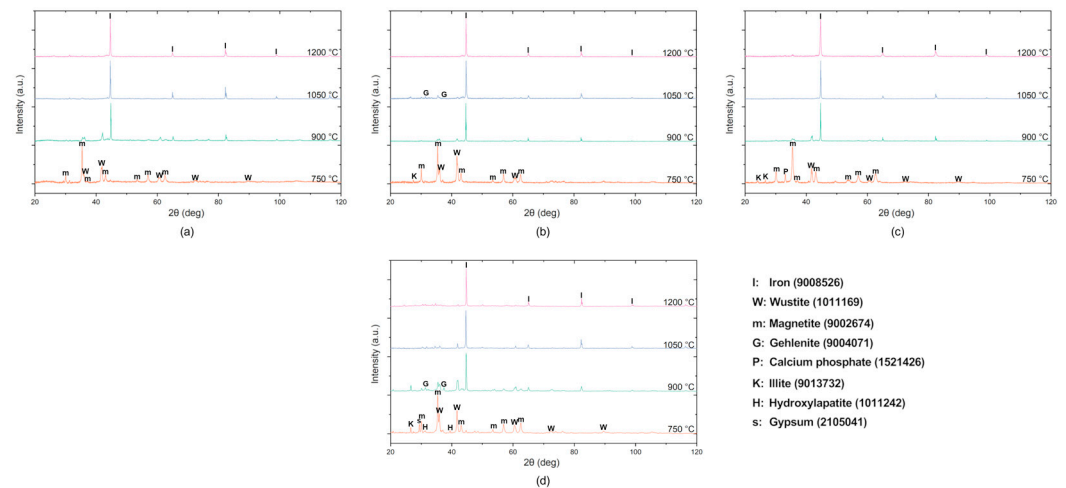


Figure 3. XRD pattern of the (a) MS/WC, (b) MS/OP750, (c) MS/OP350, and (d) MS/HC briquette after heating at 750, 900, 1050, and 1200 °C under Ar atmosphere (DB card number in parenthesis).

The XRD patterns showed a similar trend of the main reduction process (iron oxides to metallic iron) regardless of the reducing agent used. The MS/WC sample reduced at 750 °C was characterized by the presence of magnetite (Fe_3O_4) and wustite (FeO) only. Further to the latter, traces of illite ($\text{KAl}_2\text{Si}_4\text{O}_{10}(\text{OH})_2$), calcium phosphate ($\text{Ca}_3(\text{PO}_4)_2$), hydroxyapatite ($\text{Ca}_5(\text{PO}_4)_3\text{OH}$), and gypsum ($\text{CaSO}_4 \cdot 2\text{H}_2\text{O}$) were observed in the MS/OP750, MS/OP350, and MS/HC briquettes and attributed to the decomposition/reaction between the compounds contained in the ash of the reducing agent and the minor elements of

MS. It is, however, of high interest to highlight that the MS/HC sample was the only one characterized by the presence of the iron peak, whose presence was attributed to the iron oxide reduction by the high amount of volatile contained in the recipe [35]. Though the presence of residual iron oxides, mainly in the form of wustite, was still observed at 900 °C, already at this temperature, the main diffraction peaks were those attributed to the metallic iron, highlighting the start of the reduction process. Furthermore, the presence of gehlenite ($\text{Ca}_2\text{Al}_2\text{SiO}$) in the MS/HC spectrum was due to the illite decomposition, at temperatures above 800 °C, and its catalyzing effect towards the calcining of gypsum [68,69]. Finally, at 1050 °C and 1200 °C, all the reduction patterns were characterized by the presence of metallic iron as the main iron phase, with traces of unreduced iron oxides associated either with post-reduction oxidation of the samples or with an incomplete reduction of the samples, mainly evident in the MS/WC and MS/HC samples.

The samples' swelling, mass loss, and DoR after heating at 750, 900, 1050, and 1200 °C under Ar atmosphere are shown in Figure 4. To better highlight the role of the physicochemical properties of the reducing agents on the metallurgical performance, the percentage of C_{tot} , volatile matter, and ash present in each recipe as well as the specific activation energy were reported in the graphs, too.

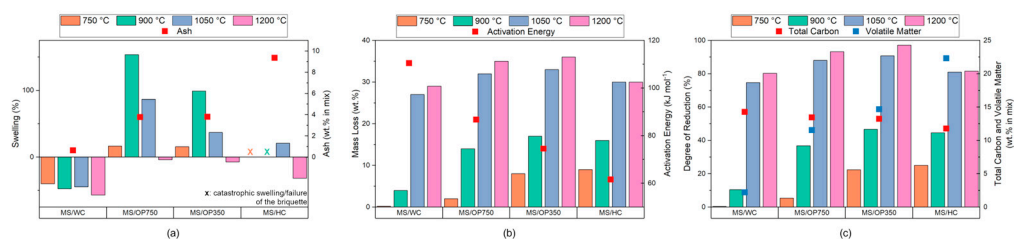


Figure 4. Comparison of the briquettes (a) swelling, (b) mass loss, and (c) degree of reduction after heating at 750, 900, 1050, and 1200 °C and effect of the specific reducing agent physicochemical properties.

The swelling behavior of the four briquette recipes (Figure 4a) agreed with the phenomenological description advanced by Reddy et al. [70]. Indeed, although the swelling is typically associated with (1) the transition from the highest to the lowest oxidation state of iron (Fe_2O_3 to FeO), (2) the reduction from wustite to metallic iron, and (3) the growth of such reduced iron fibers (whiskers), the evolution of slag and gases plays a key role in the swelling of the self-reducing aggregates [71]. Specifically, the slag evolution is intrinsically linked to the amount and chemical composition of the reducing agent ash, with alkali metal oxides (e.g., K_2O and Na_2O) considered to be the most detrimental to swelling behavior even when present in low percentages [51,70].

The MS/WC briquette was the only one characterized by negative swelling (shrinkage) regardless of heat treatment temperature, due to the almost null amount of ash. Furthermore, both the overall shrinkage trends and values corresponded to those observed by Reddy et al. [70] during the reduction of iron ore composites and spent mushroom substrate, with an increase in shrinkage between 750 and 900 °C (−40.02 and −47.55%), followed by a relative minimum at 1050 °C (−44.70%), and a final shrinkage once heated to 1200 °C (−56.92%). In contrast, in both MS/OP750 and MS/OP350, the potassium oxide liberation from the illite decomposition, as well as CO evolution due to MS reduction, increased the swelling value of the agglomerates from normal at 750 °C to abnormal at 900 °C. The higher value of the MS/OP750 briquette (153.62%) at 950 °C compared with that of MS/OP350 (99.02%) was associated with a higher concentration of potassium in the starting ash as well as the growth of a higher number of iron whiskers inside the agglomerate [43,71]. The increase in temperature allowed the sintering of reduced iron fibers in the MS/OP750 and MS/OP350 samples and the subsequent decrease in swelling at 1050 °C to shrinkage at 1200 °C (from 86.72 to −4.12% and 37.04 to −7.37%, respectively). Finally, the MS/HC briquette suffered most from the presence of alkali oxide and gas evolution during heating, undergoing catastrophic swelling at both 750 and 900 °C that caused the sample to fail at

the end or even during heating. The small swelling of the MS/HC briquette at 1050 °C (20.73%) was associated with the lower amount of nucleated iron whiskers, as evidenced by the presence of wustite in the corresponding diffraction pattern, and hence the lower stresses against the briquette walls during their growth (Figure 3d).

Both the mass loss (Figure 4b) and the DoR (Figure 4c) followed a similar trend, allowing to interchange them for the description of the reduction behavior of the sample in the 750–1200 °C range. Specifically, the higher the temperature the higher the respective value; furthermore, considering the nature of the briquette recipes studied, the transformation of iron oxide to metallic iron is the main contributor to the mass loss (Figure 3). Accordingly, the significant mass loss observed at 750 °C only for the MS/OP350 and MS/HC briquettes (8.40 and 9.15%) was attributed to the gasification reactions occurring during heating [34,43]. This was especially evident when comparing the former with the MS/OP750 sample, which despite having an amount of volatile matter and C_{tot} in the recipe close to that of MS/OP350, the higher activation energy of the OP750 inhibited the initiation of gasification resulting in a lower mass loss (1.96%). In contrast, the MS/WC sample was considered a control case because of its almost null value of volatiles, which resulted in almost no mass loss (0.13%). Although, the shift from the reduction control by gas/volatile matter to carbon (occurring between 750 and 900 °C) was responsible for an appreciable mass loss of the MS/WC and MS/OP750 briquettes (1.96 and 13.65%), the former was still characterized by the lowest value due to the higher activation energy that inhibited the complete conversion of iron oxides, as confirmed by the presence of the wustite peaks in the corresponding diffraction pattern at 900 °C (Figure 3a) [72,73]. On the other hand, in the 900–1050 °C range, the WC was properly activated and able to carry out the oxide reduction with a sixfold increase in MS/WC mass loss, whereas the remaining briquettes increased their value twofold. Finally, a slight increase (<10%) in mass loss was observed at 1200 °C, regardless of the reducing agent used, with a final value in the 29–36% range, confirming the small appreciable difference between 1050 and 1200 °C from a mineralogical point of view.

To better highlight the sigmoidal trend of the DoRs versus the temperature (Figure 4c), the values were plotted together using a modified Avrami solution of the sigmoidal function [74], in which the time parameter was replaced by the reduction temperature (expressed in degrees Kelvin), and working under the assumption that the specific DoR reached the maximum value attainable in each thermal treatment, the linearized form plot is shown in Figure 5a. Furthermore, although the use of kinetic models to describe the behavior of the self-reducing agglomerate has been explored in the literature, to the authors knowledge, there are currently no studies on the correlation of the physicochemical properties of the reducing agent with respect to the model regression parameters [75,76]. Therefore, in this work, an attempt was made to correlate them to the amount of volatile matter and fixed carbon in each recipe. Specifically, the former was plotted against the constant parameter (k) and the latter against the slope of the regression curve (n); the plots are shown in Figures 5b and 5c, respectively.

Each regression curve showed a linear correlation coefficient (R-square) greater than 0.90, confirming the sigmoidal trend of DoR versus temperature. Similarly, the R-squares of volatile matter and fixed carbon with respect to $\ln(k)$ and n were close to unity (0.96 and 0.98, respectively), further emphasizing their role on the proceeding in the reduction of mill scale agglomerates. On the one hand, the higher the volatile matter, the higher the regression constant and the DoR at low temperature due to gasification (below 1050 °C in this study); on the other hand, the higher the fixed carbon, the higher the slope of the regression curve and the ability to recover iron at high temperatures (above 1050 °C in this study).

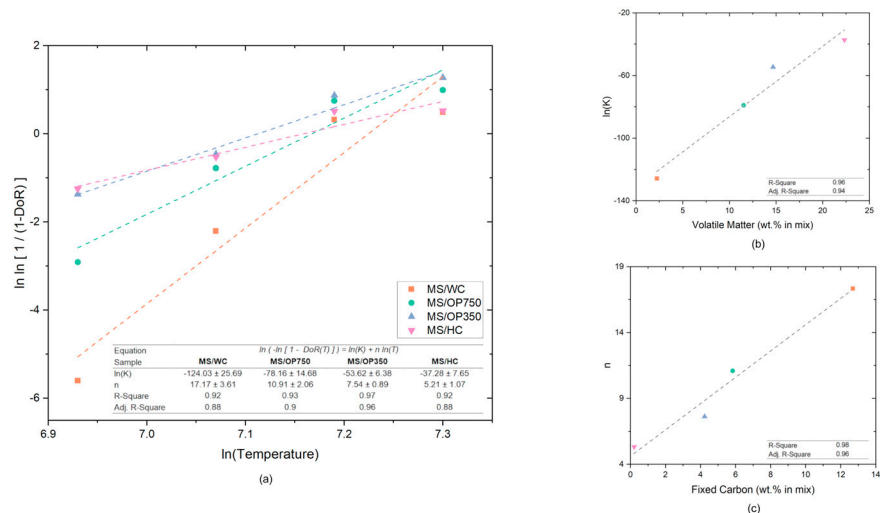


Figure 5. (a) Linearized form plots of the degree of reduction versus temperature, and relationship between (b) the regression constant and volatile matter in the recipe, and (c) the regression curve slope and fixed carbon in the recipe.

Smelting Behavior, Iron Recovery, and Industrial Transferability

Following the main purpose of extractive metallurgy, consisting of the recovery of valuable metals from metal-containing ores or sources and aiming at obtaining a secondary raw material in the form of clean iron to be reintroduced as additional feedstock into the main steelmaking furnaces, the four recipes thermally were treated at 1400 °C under Ar atmosphere for 15 min to evaluate their smelting behavior.

The visual appearance and metallography analysis of the samples after smelting is given in Figure 6. If the briquette was not able to achieve a full smelting, a metallographic preparation was carried out to expose the cross section, which was considered as most representative for evaluating the reduction morphology and porosity distribution.

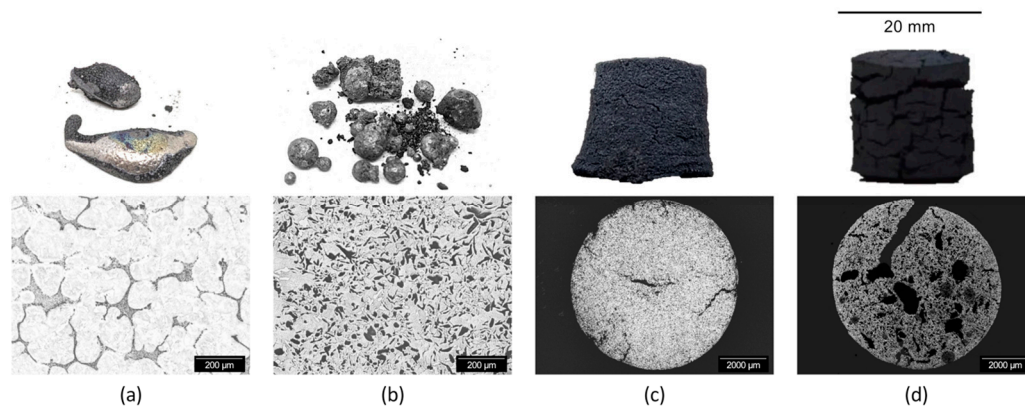


Figure 6. Visual appearance and metallographic analysis of the (a) MS/WC, (b) MS/OP750, (c) MS/OP350, and (d) MS/HC briquettes treated at 1400 °C.

On the one hand, the MS/WC and MS/OP750 samples were able to achieve a proper melting with a final microstructure typical of class III_{ISO} and V_{ISO} cast irons, respectively [77]. On the other hand, the MS/OP350 and MS/HC briquettes retained the agglomerated shape with a shrinkage of 65.84 and 57.25%, as well as a morphology similar to that observed by Sohn and Fruehan [78] following iron ore reduction by coal devolatilization. It is therefore interesting to further relate the slopes of the DoR regression curve (Figure 5c) to the smelting behavior of the briquettes. Based on the results, it can be stated that the heat treatment at 1400 °C of agglomerates with an n value (in the 750–1200 °C range) greater than 10.91 allows their smelting as well as the nucleation and growth of graphite flakes,

with higher n values leading to coarser recovered iron droplets (Figure 6a,b), while the lower the value with respect to the threshold, the greater the amount of porosity and cavities left by gas evolution during the reduction process, and the less sintering and shrinkage (Figure 6c,d). Furthermore, the mass losses perfectly followed the amount of fixed carbon in the mixture, highlighting once again its major contribution at high thermal treatment temperatures. In ascending order, the values obtained were 36.58, 38.93, 40.24, and 46.27 percent from the MS/HC, MS/OP350, MS/OP750, and MS/WC samples, respectively.

SEM-EDS analysis was used to highlight the presence of harmful elements dispersed in the recovered iron matrix (e.g., P and S) and the chemical composition of the slag, with the latter only investigated for MS/OP350 and MS/HC briquettes; the micrographs are shown in Figure 7.

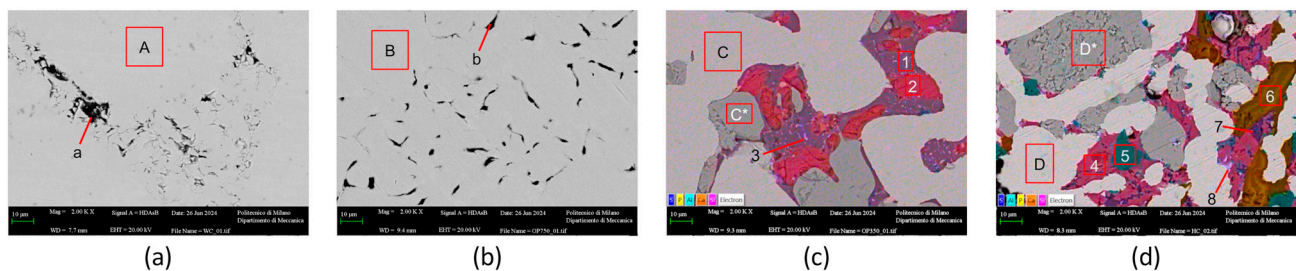


Figure 7. SEM micrograph of the (a) MS/WC and (b) MS/OP750 briquettes and SEM-EDS map of the cross section of the (c) MS/OP350 and (d) MS/HC briquettes.

SEM observation of the cross section associated with the EDS spectra (Table 5) confirmed the presence of graphite in the MS/WC and MS/OP750 iron matrices (Figure 7a,b), as well as the absence of sulfur and phosphorus in the latter, allowing the direct introduction of the reduced iron into metallurgical furnaces as secondary raw material for bath dilution without the need for substantial process modification or the risk of introducing harmful elements into the melt [79]. The SEM-EDS maps of the MS/OP350 and MS/HC briquettes (Figure 7c,d) showed a microstructure characterized by the presence of uniformly distributed islands of reduced and unreduced iron oxides throughout the surface, strongly linked to the slag phase. In particular, the MS/OP350 slag was characterized by a matrix of gehlenite together with calcium-olivine (Ca_2SiO_4) and secondarily precipitated crystals of iron-gehlenite ($\text{Ca}_2\text{FeAlSiO}_7$), within which phosphorus and sulfur were dissolved, resembling the mineralogy of high basicity BOF slags and that of self-reduced briquettes of flue dust and mill scale [80–82]. Further to gehlenite, a solid solution of olivine, kirschenite (CaFeSiO_4), iron-alumina spinel ($\text{FeO}\cdot\text{Al}_2\text{O}_3$), calcium phosphate ($\text{Ca}_3(\text{PO}_4)_2$), which is derived from the thermal decomposition of hydroxyapatite [83], and iron sulfide (FeS) constituted the mineralogy of the MS/HC sample slag.

From a practical point of view, the DoM achieved by the MS/WC, MS/OP750, and MS/OP350 briquettes (100, 100, and 82.32%, respectively), as well as the slag mineralogy of the latter, would allow their direct introduction into the main metallurgical furnaces as secondary raw material without affecting the specific process times and/or bath chemistries [45].

In contrast, the low DoM achieved by the MS/HC briquette (66.79%) would require a higher treatment temperature to achieve adequate iron recovery and be in line with the productivity constraints of metallurgical furnaces. For example, the DoM of self-reducing briquettes composed of iron ore fines, flue dust, and BOF/BF sludge increased from 69.70 to 97.95% when they were treated at 1500 instead of 1400 °C [84]. This temperature is achieved in BF, EAF, and cupola furnaces and would also be advantageous for the removal of sulfides observed in MS/HC briquette slag, as it would increase the desulfurization capacity of the slag itself, thus avoiding the need for a desulfurization agent after iron tapping/recasting (increased process costs) or a longer desulfurization period (increased process time) [85].

Table 5. EDS spectra of MS/WC, MS/OP750, MS/OP350, and MS/HC briquettes expressed in wt.% (A–D, C*–D* and a–b spectra are given as average values in the same phase).

Spectrum	C	O	Al	Si	P	S	Ca	Fe	Phase
A–D	3.57 ^a							96.43	Iron
C*–D*		24.24						75.76	Wustite
a–b	75.99	1.20						22.81	Graphite
1		38.83	14.05	11.54			27.55	8.03	Gehlenite
2		38.29		15.95			39.71	6.05	Calcio-olivine
3		37.39	2.82	15.56	0.2	0.71	24.41	18.91	Ferri-gehlenite
4		38.52		14.52	1.16		19.01	26.8	Kirschenite
5		34.17	22.87					42.96	Spinel
6		44.66			19.45		33.73	2.16	Calcium phosphate
7		44.66	18.12	10.33	4.18		11.49	11.23	Gehlenite
8		4.27		1.21		35	1.02	58.51	Iron sulfide

^a Carbon derives from the iron carburization in the MS/WC and MS/OP750 samples.

Finally, considering the potential benefits that MS reduction through biogenic carbon would bring at the national level, the MS/OP750 recipe is the most promising. Indeed, the Italian olive production sector is the second largest in the world, with a crucial economic and social role in the southern regions, and is responsible for about 3 Mton of olive pomace per year as the main by-product; the latter is currently used as an energy source in incineration plants with unsatisfactory results, thus requiring the need for more promising valorization paths [86–88]. It is therefore possible to estimate that the creation of such a symbiosis of steel-agricultural waste valorization would not only have the potential to cover 18.70% of the 1.86 Mton of clean iron sources currently imported to Italy per year (updated data to 2022) [89], in the case of using the entire annual availability of mill scale, but also valorize 433 kton of raw pomace, with the latter being needed to achieve the 130 kton of OP750 (given a solid pyrolysis yield of 0.3 at 750 °C) to be agglomerated with MS as the reducing agent.

4. Conclusion

Aiming to deepen the knowledge of the role of physicochemical properties of biogenic carbon when agglomerated with mill scale, this work investigated the mechanical and metallurgical performance of four different recipes of self-reducing briquettes with increasing amounts of volatile matter and ash, as well as the parallel decrease of fixed carbon.

The main results of the present study can be summarized as follows:

- The mechanical performance are indirectly controlled by the hydrophilicity or hydrophobicity of the reducing agents used. Hydrophilic biogenic carbon allows the obtaining of agglomerates characterized by smooth surfaces and are highly packed, whereas hydrophobic biogenic carbon enhances the water expulsion from the agglomerate during the curing period leading to the formation of several cracks that inhibit the overall mechanical resistance, acting as low-resistance points. Still, the values achieved were comparable to or even better than that of pellets typically used in shaft furnaces (e.g., survival of 7 drops, CCS of 9.5 MPa, bulk density of 2 g cm⁻³).
- The iron recovery is regulated by the amount of fixed carbon and volatile matter in the agglomerate. Specifically, though the briquetting is able to exploit the reduction of the iron oxides from the volatiles at 750 °C onward, even in the case of nearly null fixed carbon, an amount higher than 6.93% of fixed carbon and lower than 11.55% of volatile matter is required to fully recover the iron oxides of the agglomerate at 1400 °C, with a final microstructure associable to that of cast irons. Lower amounts of fixed carbon and higher volatile matter lead to the maintenance of the agglomerate morphology with the coexistence of reduced and unreduced iron as well as slag.
- The presence of alkali in the ash is highly detrimental for the agglomerates once immersed due to their dissolution and catalyzing effect towards the calcite hydration

which leads to briquette failure within 600 s. Furthermore, during heating, even a small amount of alkali can enhance the swelling in the 750–1050 °C range up to catastrophic values. Nevertheless, the presence of Ca-, Al-, and Si- compounds in the reducing agent ash allows the creation of a steelmaking close slag at 1400 °C, able to trap most of the phosphorus and sulfur, and protecting the recovered iron.

- Among the four biogenic carbon matrices, the use of wood chips or olive pomace pyrolyzed at 750 °C appears to be the most promising to recover the iron from mill scale and directly reintroduce it as secondary raw material in metallurgical furnaces when reduced at 1400 °C. On the contrary, slag separation processes and/or higher treatment temperatures are required for the recipes exploiting olive pomace pyrolyzed at 350 °C and hydrothermally carbonized sewage sludge to enhance the degree of metallization achieved (82.32% and 66.79%) up to industrial usable levels.

In conclusion, taking into account the future challenge for the valorization of mill scale that will arise due to the depletion of sintering plants and the shift to more electricity-focused iron and steel production, the agglomeration of such residue together with biogenic carbon sources could be a more than viable alternative solution for the recovery of the iron contained therein. Consequently, the next questions to be addressed will have to focus on understanding: (i) the optimal briquette charging conditions (e.g., quantity, time, relative position in the bucket, as unreduced or reduced) in the main furnaces (e.g., EAF, ESF, and BOF); (ii) any changes in the reduction behavior of virgin briquettes once interacting with the other charging materials, slag, and process period (reducing or oxidizing); and, most importantly, (iii) any alteration in the quality of the molten steel and the productivity of the furnaces themselves.

5. Patents

The experimental results shown and discussed in the present manuscript led to the setup of a process described and deposited in patent n. WO 2024/013653 A1 [90].

Supplementary Materials: The following supporting information can be downloaded at: <https://www.mdpi.com/article/10.3390/met14080882/s1>, Figure S1: XRD pattern of the mill scale; Figure S2: XRD patterns of the reducing agents (a) WC, (b) OP750, (c) OP350 and (d) HC; Figure S3: Temporal evolution of the (a) MS/WC, (b) MS/OP750, (c) MS/OP350 and (d) MS/HC briquettes during the water immersion resistance test.

Author Contributions: Conceptualization, G.D., D.M. and C.M.; methodology, G.D.; software, G.D. and S.S.; validation, G.D. and S.S.; formal analysis, G.D., D.M. and S.S.; investigation, G.D. and D.M.; resources, G.D. and S.S.; data curation, G.D. and D.M.; writing—original draft preparation, G.D.; writing—review and editing, G.D., D.M., S.S. and C.M.; visualization, G.D. and S.S.; supervision, D.M. and C.M. All authors have read and agreed to the published version of the manuscript.

Funding: (Italian version) Gli interventi oggetto della presente procedura sono finanziati a valere sulle risorse previste dal PNRR Missione 4 (“Istruzione e ricerca”)—Componente 2 (“MICS-3A-ITALY-SPOKE 4”)—Investimento 1.3 (“Partenariato Esteso Made in Italy Circolare e Sostenibile 3A-ITALY—Spoke 4 Smart and sustainable materials for circular and augmented industrial products and processes”), PE0000004, finanziato dall’Unione Europea-NextGenerationEU—CUP D43C22003120001. (English version) This study has been financed from the resources provided by the PNRR Mission 4 (“Education and Research”)—Component 2 (“MICS-3A-ITALY-SPOKE 4”)—Investment 1.3 (“Expanded Partnership Made in Italy Circular and Sustainable 3A-ITALY—Spoke 4 Smart and sustainable materials for circular and augmented industrial products and processes”), PE000004, funded by the European Union-NextGenerationEU—CUP D43C22003120001.

Data Availability Statement: The data presented in this study are available on request from the corresponding author (accurately indicate status).

Conflicts of Interest: The authors declare no conflicts of interest.

References

1. Liu, Y.; Li, H.; Huang, S.; An, H.; Santagata, R.; Ulgiati, S. Environmental and Economic-Related Impact Assessment of Iron and Steel Production. A Call for Shared Responsibility in Global Trade. *J. Clean. Prod.* **2020**, *269*, 122239. [CrossRef]
2. World Steel Association. *World Steel in Figures 2023*; World Steel Association: Bruxelles, Belgium, 2023.
3. International Energy Agency. *Iron and Steel Technology Roadmap*; International Energy Agency: Paris, France, 2020.
4. Dall'Osto, G.; Mombelli, D.; Mapelli, C. Consequences of the Direct Reduction and Electric Steelmaking Grid Creation on the Italian Steel Sector. *Metals* **2024**, *14*, 311. [CrossRef]
5. Colla, V.; Branca, T.A.; Pietruck, R.; Wölfelschneider, S.; Morillon, A.; Algermissen, D.; Rosendahl, S.; Granbom, H.; Martini, U.; Snaet, D. Future Research and Developments on Reuse and Recycling of Steelmaking By-Products. *Metals* **2023**, *13*, 676. [CrossRef]
6. BAT. *Best Available Techniques—Reference Document for Iron and Steel Production: Industrial Emissions Directive 2010/75/EU: Integrated Pollution Prevention and Control*; Joint Research Centre of the European Commission: Brussels, Belgium, 2012.
7. Iluțiu-Varvara, D.-A.; Aciu, C.; Tintelecan, M.; Sas-Boca, I.-M. Assessment of Recycling Potential of the Steel Mill Scale in the Composition of Mortars for Sustainable Manufacturing. *Procedia Manuf.* **2020**, *46*, 131–135. [CrossRef]
8. Spiliotis, X.; Ntampeglotis, K.; Kasiteropoulou, D.; Lamprakopoulos, S.; Lolos, K.; Karayannis, V.; Papapolymerou, G. Valorization of Mill Scale Waste by Its Incorporation in Fired Clay Bricks. *Key Eng. Mater.* **2014**, *608*, 8–13. [CrossRef]
9. Touzi, N.; Horchani-Naifer, K. A Study on the Preparation and Characterization of Pigment Quality from Mill Scale Steel Wastes. *Environ. Sci. Pollut. Res.* **2023**, *31*, 40538–40553. [CrossRef]
10. Iluțiu-Varvara, D.-A.; Aciu, C.; Maria Mărza, C.; Sas-Boca, I.-M.; Tintelecan, M. Assessment of Recycling Potential of the Oily Mill Scale in the Steelmaking Industry. *Procedia Manuf.* **2018**, *22*, 228–232. [CrossRef]
11. Khodakovskii, V.R.; Zhorniyak, A.F. Estimate of the Supply of Mill Scale for the Manufacture of Iron Powders. *Sov. Powder Metall. Met. Ceram.* **1965**, *4*, 505–510. [CrossRef]
12. Manukyan, N.V. Carbide-Thermic Method of Preparation of Iron Powder. *Sov. Powder Metall. Met. Ceram.* **1967**, *6*, 260–263. [CrossRef]
13. Eissa, M.; Ahmed, A.; El-Fawkhry, M. Conversion of Mill Scale Waste into Valuable Products via Carbothermic Reduction. *J. Metall.* **2015**, *2015*, 1–9. [CrossRef]
14. Martín, M.I.; López, F.A.; Torralba, J.M. Production of Sponge Iron Powder by Reduction of Rolling Mill Scale. *Ironmak. Steelmak.* **2012**, *39*, 155–162. [CrossRef]
15. Cho, S.; Lee, J. Metal Recovery from Stainless Steel Mill Scale by Microwave Heating. *Met. Mater. Int.* **2008**, *14*, 193–196. [CrossRef]
16. Bugdayci, M.; Alkan, M.; Turan, A.; Yücel, O. Production of Iron Based Alloys from Mill Scale through Metallothermic Reduction. *High Temp. Mater. Process.* **2018**, *37*, 889–898. [CrossRef]
17. Kallio, M. Use of the Aluminothermic Reaction in the Treatment of Steel Industry By-Products. *J. Mater. Synth. Process.* **2000**, *8*, 87–92. [CrossRef]
18. Khanna, R.; Konyukhov, Y.; Li, K.; Jayasankar, K.; Maslennikov, N.; Zinoveev, D.; Kargin, J.; Burmistrov, I.; Leybo, D.; Kravchenko, M.; et al. Innovative Transformation and Valorisation of Red Mill Scale Waste into Ferroalloys: Carbothermic Reduction in the Presence of Alumina. *Sustainability* **2023**, *15*, 16810. [CrossRef]
19. Benchiheub, O.; Mechachti, S.; Serrai, S.; Khalifa, M.G. Elaboration of Iron Powder from Mill Scale. *J. Mater. Environ. Sci.* **2010**, *1*, 267–276.
20. Bagatini, M.C.; Zymła, V.; Osório, E.; Vilela, A.C.F. Characterization and Reduction Behavior of Mill Scale. *ISIJ Int.* **2011**, *51*, 1072–1079. [CrossRef]
21. Gaballah, N.M.; Zikry, A.F.; Khalifa, M.G.; Farag, A.B.; El-Hussiny, N.A.; Shalabi, M.E.H. Production of Iron from Mill Scale Industrial Waste via Hydrogen. *Open J. Inorg. Non-Met. Mater.* **2013**, *03*, 23–28. [CrossRef]
22. Domalski, E.S.; MacCrehan, W.A.; Moody, J.R.; Tewari, Y.B.; Walker, J.A. Characterization of Millscale Steel Wastes. National Bureau of Standards: Washington, DC, USA, 1983.
23. Umadevi, T.; Brahmacharyulu, A.; Karthik, P.; Mahapatra, P.C.; Prabhu, M.; Ranjan, M. Recycling of Steel Plant Mill Scale via Iron Ore Sintering Plant. *Ironmak. Steelmak.* **2012**, *39*, 222–227. [CrossRef]
24. Biochar for a Sustainable EAF Steel Production (GREENEAF2)—Publications Office of the EU. Available online: <https://op.europa.eu/en/publication-detail/-/publication/7198c147-22b2-11e9-8d04-01aa75ed71a1/language-en> (accessed on 6 July 2023).
25. Sustainable EAF Steel Production (GREENEAF)—Publications Office of the EU. Available online: <https://op.europa.eu/en/publication-detail/-/publication/e7dc500c-82de-4c2d-8558-5e24a2d335fb/language-en> (accessed on 6 July 2023).
26. Meier, T.; Hay, T.; Echterhof, T.; Pfeifer, H.; Rekersdrees, T.; Schlinge, L.; Elsabagh, S.; Schliephake, H. Process Modeling and Simulation of Biochar Usage in an Electric Arc Furnace as a Substitute for Fossil Coal. *Steel Res. Int.* **2017**, *88*, 1600458. [CrossRef]
27. He, X.-M.; Yi, S.; Fu, P.-R.; Zeng, X.-C.; Zhang, D.; Cheng, X.-H. Combustion Reactivity of Biochar and Char Generated from Co-Pyrolysis of Coal and Four Additives: Application in Blast Furnace. *J. Energy Eng.* **2017**, *143*, 04016023. [CrossRef]
28. Robinson, R.; Brabie, L.; Pettersson, M.; Amovic, M.; Ljunggren, R. An Empirical Comparative Study of Renewable Biochar and Fossil Carbon as Carburizer in Steelmaking. *ISIJ Int.* **2022**, *62*, 2522–2528. [CrossRef]
29. Cardarelli, A.; De Santis, M.; Cirilli, F.; Barbanera, M. Computational Fluid Dynamics Analysis of Biochar Combustion in a Simulated Ironmaking Electric Arc Furnace. *Fuel* **2022**, *328*, 125267. [CrossRef]

30. DiGiovanni, C.; Li, D.; Ng, K.W.; Huang, X. Ranking of Injection Biochar for Slag Foaming Applications in Steelmaking. *Metals* **2023**, *13*, 1003. [[CrossRef](#)]
31. Echterhof, T. Review on the Use of Alternative Carbon Sources in EAF Steelmaking. *Metals* **2021**, *11*, 222. [[CrossRef](#)]
32. Safarian, S. To What Extent Could Biochar Replace Coal and Coke in Steel Industries? *Fuel* **2023**, *339*, 127401. [[CrossRef](#)]
33. Konishi, H.; Ichikawa, K.; Usui, T. Effect of Residual Volatile Matter on Reduction of Iron Oxide in Semi-Charcoal Composite Pellets. *ISIJ Int.* **2010**, *50*, 386–389. [[CrossRef](#)]
34. Wei, R.; Cang, D.; Bai, Y.; Huang, D.; Liu, X. Reduction Characteristics and Kinetics of Iron Oxide by Carbon in Biomass. *Ironmak. Steelmak.* **2016**, *43*, 144–152. [[CrossRef](#)]
35. Bagatini, M.C.; Kan, T.; Evans, T.J.; Strezov, V. Iron Ore Reduction by Biomass Volatiles. *J. Sustain. Metall.* **2021**, *7*, 215–226. [[CrossRef](#)]
36. El-Tawil, A.; Ahmed, H.M.; El-Geassy, A.A.; Bjorkman, B. Effect of Volatile Matter on Reduction of Iron Oxide-Containing Carbon Composite. In Proceedings of the 54th Annual Conference of Metallurgists (COM 2015), Fairmont Royal York, Toronto, ON, Canada, 8 August 2015; pp. 1–14.
37. Das, D.; Anand, A.; Gautam, S.; Rajak, V.K. Assessment of Utilization Potential of Biomass Volatiles and Biochar as a Reducing Agent for Iron Ore Pellets. *Environ. Technol.* **2024**, *45*, 158–169. [[CrossRef](#)]
38. Sönmez, İ.; Şahbudak, K. Optimization of Sponge Iron (Direct Reduced Iron) Production with Box-Wilson Experimental Design by Using Iron Pellets and Lignite as Reductant. *Rev. Metal.* **2023**, *59*, e241. [[CrossRef](#)]
39. Murakami, T.; Takahashi, T.; Fuji, S.; Maruoka, D.; Kasai, E. Development of Manufacturing Principle of Porous Iron by Carbothermic Reduction of Composite of Hematite and Biomass Char. *Mater. Trans.* **2017**, *58*, 1742–1748. [[CrossRef](#)]
40. Liu, Z.; Bi, X.; Gao, Z.; Liu, W. Carbothermal Reduction of Iron Ore in Its Concentrate-Agricultural Waste Pellets. *Adv. Mater. Sci. Eng.* **2018**, *2018*, 1–6. [[CrossRef](#)]
41. Chuanchai, A.; Wu, K.-T. Potential of Pinewood Biochar as an Eco-Friendly Reducing Agent in Iron Ore Reduction. *ACS Omega* **2024**, *9*, 14279–14286. [[CrossRef](#)] [[PubMed](#)]
42. Ubando, A.T.; Chen, W.-H.; Ong, H.C. Iron Oxide Reduction by Graphite and Torrefied Biomass Analyzed by TG-FTIR for Mitigating CO₂ Emissions. *Energy* **2019**, *180*, 968–977. [[CrossRef](#)]
43. Vitikka, O.; Iljana, M.; Heikkilä, A.; Tkalenko, I.; Kovtun, O.; Koriuchev, N.; Shehovsov, D.; Fabritius, T. Effect of Biocarbon Addition on Metallurgical Properties of Mill Scale-Based Auger Pressing Briquettes. *ISIJ Int.* **2024**, *64*, 964–977. [[CrossRef](#)]
44. Khaerudini, D.S.; Chanif, I.; Insiyanda, D.R.; Destyorini, F.; Alva, S.; Pramono, A. Preparation and Characterization of Mill Scale Industrial Waste Reduced by Biomass-Based Carbon. *J. Sustain. Metall.* **2019**, *5*, 510–518. [[CrossRef](#)]
45. Bagatini, M.C.; Zymla, V.; Osório, E.; Vilela, A.C.F. Scale Recycling Through Self-Reducing Briquettes to Use in EAF. *ISIJ Int.* **2017**, *57*, 2081–2090. [[CrossRef](#)]
46. Dall’Osto, G.; Mombelli, D.; Pittalis, A.; Mapelli, C. Biochar and Other Carbonaceous Materials Used in Steelmaking: Possibilities and Synergies for Power Generation by Direct Carbon Fuel Cell. *Biomass Bioenergy* **2023**, *177*, 106930. [[CrossRef](#)]
47. ASTM D1762-84; American Society for Testing and Materials International Standard Test Method for Chemical Analysis of Wood Charcoal. ASTM: Conshohocken, PA, USA, 2009.
48. Lim, A.C.R.; Chin, B.L.F.; Jawad, Z.A.; Hii, K.L. Kinetic Analysis of Rice Husk Pyrolysis Using Kissinger-Akahira-Sunose (KAS) Method. *Procedia Eng.* **2016**, *148*, 1247–1251. [[CrossRef](#)]
49. Hussain, R.; Ghosh, K.K.; Garg, A.; Ravi, K. Effect of Biochar Produced from Mesquite on the Compaction Characteristics and Shear Strength of a Clayey Sand. *Geotech. Geol. Eng.* **2021**, *39*, 1117–1131. [[CrossRef](#)]
50. Mombelli, D.; Dall’Osto, G.; Trombetta, V.; Mapelli, C. Comparison of the Reduction Behavior through Blast Furnace Sludge of Two Industrial Jarosites. *J. Environ. Chem. Eng.* **2023**, *11*, 109360. [[CrossRef](#)]
51. Dall’Osto, G.; Mombelli, D.; Trombetta, V.; Mapelli, C. Effect of Particle Size and Starch Gelatinization on the Mechanical and Metallurgical Performance of Jarosite Plus Blast Furnace Sludge Self-Reducing Briquettes. *J. Sustain. Metall.* **2024**, *10*, 759–774. [[CrossRef](#)]
52. Mombelli, D.; Gonçalves, D.L.; Mapelli, C.; Barella, S.; Gruttadauria, A. Processing and Characterization of Self-Reducing Briquettes Made of Jarosite and Blast Furnace Sludges. *J. Sustain. Metall.* **2021**, *7*, 1603–1626. [[CrossRef](#)]
53. ASTM D440-07; American Society for Testing and Materials International Standard Test Method of Drop Shatter Test for Coal. ASTM: Conshohocken, PA, USA, 2019.
54. BS ISO 4700:2015; Iron Ore Pellets for Blast Furnace and Direct Reduction Feedstocks—Determination of the Crushing Strength. ISO: Geneva, Switzerland, 2015.
55. Richards, S.R. Physical Testing of Fuel Briquettes. *Fuel Process. Technol.* **1990**, *25*, 89–100. [[CrossRef](#)]
56. BS ISO 11258:2015; Iron Ores for Shaft Direct-Reduction Feedstocks. Determination of the Reducibility Index, Final Degree of Reduction and Degree of Metallization. ISO: Geneva, Switzerland, 2015.
57. Leino, T.; Taskinen, P.; Eric, R.H. Determination of Metallization Degree of Pre-Reduced Chromite with Image and Rietveld Analysis. *J. Min. Metall. Sect. B Metall.* **2020**, *56*, 289–297. [[CrossRef](#)]
58. Li, Z.; Zou, H. Optimization of Biomass Fuel Cold Briquetting Parameters Based on Response Surface Analysis. *J. Inst. Eng. (India) Ser. C* **2022**, *103*, 459–472. [[CrossRef](#)]
59. Seetharaman, S.; Teng, L.; Hayashi, M.; Wang, L. Understanding the Properties of Slags. *ISIJ Int.* **2013**, *53*, 1–8. [[CrossRef](#)]

60. Seetharaman, S. *Treatise on Process Metallurgy, Volume 3: Industrial Processes*; Elsevier: Amsterdam, The Netherlands, 2013; Volume 3.
61. Zhang, C.; Zhang, N.; Pan, D.; Qian, D.; An, Y.; Yuan, Y.; Xiang, Z.; Wang, Y. Experimental Study on Sensitivity of Porosity to Pressure and Particle Size in Loose Coal Media. *Energies* **2018**, *11*, 2274. [[CrossRef](#)]
62. Pang, L.; Yang, Y.; Wu, L.; Wang, F.; Meng, H. Effect of Particle Sizes on the Physical and Mechanical Properties of Briquettes. *Energies* **2019**, *12*, 3618. [[CrossRef](#)]
63. Richards, S.R. Briquetting Peat and Peat-Coal Mixtures. *Fuel. Process. Technol.* **1990**, *25*, 175–190. [[CrossRef](#)]
64. Suarez, J.A.; Luengo, C.A. Coffee Husk Briquettes: A New Renewable Energy Source. *Energy Sources* **2003**, *25*, 961–967. [[CrossRef](#)]
65. El-Hussiny, N.A.A.; Shalabi, M.E.H.E.H. A Self-Reduced Intermediate Product from Iron and Steel Plants Waste Materials Using a Briquetting Process. *Powder Technol.* **2011**, *205*, 217–223. [[CrossRef](#)]
66. Davies, R.M.; Davies, O.A. Effect of Briquetting Process Variables on Hygroscopic Property of Water Hyacinth Briquettes. *J. Renew. Energy* **2013**, *2013*, 429230. [[CrossRef](#)]
67. Finneran, D.W.; Morse, J.W. Calcite Dissolution Kinetics in Saline Waters. *Chem. Geol.* **2009**, *268*, 137–146. [[CrossRef](#)]
68. Araújo, J.H.d.; Silva, N.F.d.; Acchar, W.; Gomes, U.U. Thermal Decomposition of Illite. *Mater. Res.* **2004**, *7*, 359–361. [[CrossRef](#)]
69. Lu, D.; Chen, Q.; Li, C.; Gong, S. Effect of Potassium Feldspar on the Decomposition Rate of Phosphogypsum. *J. Chem. Technol. Biotechnol.* **2021**, *96*, 374–383. [[CrossRef](#)]
70. Reddy, D.S.; Chang, H.-H.; Tsai, M.-Y.; Chen, I.-G.; Wu, K.-T.; Liu, S.-H. Swelling and Softening Behavior of Iron Ore-Spent Mushroom Substrate Composite Pellets during Carbothermal Reduction. *J. Mater. Res. Technol.* **2023**, *22*, 1999–2007. [[CrossRef](#)]
71. Singh, M.; Björkman, B. Effect of Reduction Conditions on the Swelling Behaviour of Cement-Bonded Briquettes. *ISIJ Int.* **2004**, *44*, 294–303. [[CrossRef](#)]
72. Sarkar, S.B.; Ray, H.S.; Chatterjee, I. Kinetics of Reduction of Iron Ore—Coal Pellets. *J. Therm. Anal.* **1989**, *35*, 2461–2469. [[CrossRef](#)]
73. Bagatini, M.C.; Zymła, V.; Osório, E.; Vilela, A.C.F. Carbon Gasification in Self-Reducing Mixtures. *ISIJ Int.* **2014**, *54*, 2687–2696. [[CrossRef](#)]
74. Fanfoni, M.; Tomellini, M. The Johnson-Mehl- Avrami-Kohnogorov Model: A Brief Review. *Il Nuovo Cimento D* **1998**, *20*, 1171–1182. [[CrossRef](#)]
75. Yuan, X.; Luo, F.; Liu, S.; Zhang, M.; Zhou, D. Comparative Study on the Kinetics of the Isothermal Reduction of Iron Ore Composite Pellets Using Coke, Charcoal, and Biomass as Reducing Agents. *Metals* **2021**, *11*, 340. [[CrossRef](#)]
76. Chai, Y.; Fan, Y.; Li, Z.; Wu, J.; Zhang, Y.; Wang, Y.; Luo, G.; An, S. Kinetics of Reduction in Stages of Pellets Prepared from the Bayan Obo Iron Ore Concentrate. *ACS Omega* **2022**, *7*, 7759–7768. [[CrossRef](#)] [[PubMed](#)]
77. Friess, J.; Sonntag, U.; Steller, I.; Bührig-Polaczek, A. From Individual Graphite Assignment to an Improved Digital Image Analysis of Ductile Iron. *Int. J. Met.* **2020**, *14*, 1090–1104. [[CrossRef](#)]
78. Sohn, I.; Fruehan, R.J. The Reduction of Iron Oxides by Volatiles in a Rotary Hearth Furnace Process: Part III. The Simulation of Volatile Reduction in a Multi-Layer Rotary Hearth Furnace Process. *Metall. Mater. Trans. B* **2006**, *37*, 231–238. [[CrossRef](#)]
79. Ghosh, A.; Chatterjee, A. *Ironmaking and Steelmaking Theory and Practice*; PHI Learning Private Limited: New Delhi, India, 2008; Volume 20, ISBN 812033289X.
80. Rietmeijer, F.J.M.; Nuth, J.A.; Pun, A. The Formation of Mg,Fe-silicates by Reactions between Amorphous Magnesiosilica Smoke Particles and Metallic Iron Nanograins with Implications for Comet Silicate Origins. *Meteorit. Planet. Sci.* **2013**, *48*, 1823–1840. [[CrossRef](#)]
81. Liu, C.; Huang, S.; Blanpain, B.; Guo, M. Effect of Al₂O₃ Addition on Mineralogical Modification and Crystallization Kinetics of a High Basicity BOF Steel Slag. *Metall. Mater. Trans. B* **2019**, *50*, 271–281. [[CrossRef](#)]
82. Bagatini, M.C.; Fernandes, T.; Silva, R.; Galvão, D.F.; Flores, I.V. Mill Scale and Flue Dust Briquettes as Alternative Burden to Low Height Blast Furnaces. *J. Clean. Prod.* **2020**, *276*, 124332. [[CrossRef](#)]
83. Böhme, N.; Hauke, K.; Dohrn, M.; Neuroth, M.; Geisler, T. High-Temperature Phase Transformations of Hydroxylapatite and the Formation of Silicocarnotite in the Hydroxylapatite–Quartz–Lime System Studied in Situ and in Operando by Raman Spectroscopy. *J. Mater. Sci.* **2022**, *57*, 15239–15266. [[CrossRef](#)]
84. Mohanty, M.K.; Mishra, S.; Mishra, B.; Sarkar, S.; Samal, S.K. A Novel Technique for Making Cold Briquettes for Charging in Blast Furnace. *IOP Conf. Ser. Mater. Sci. Eng.* **2016**, *115*, 012020. [[CrossRef](#)]
85. Mombelli, D.; Mapelli, C.; Barella, S.; Gruttadauria, A.; Spada, E. Jarosite Wastes Reduction through Blast Furnace Sludges for Cast Iron Production. *J. Environ. Chem. Eng.* **2019**, *7*, 102996. [[CrossRef](#)]
86. Valenti, F.; Arcidiacono, C.; Chinnici, G.; Cascone, G.; Porto, S.M. Quantification of Olive Pomace Availability for Biogas Production by Using a GIS-based Model. *Biofuels Bioprod. Biorefining* **2017**, *11*, 784–797. [[CrossRef](#)]
87. CREA Consiglio per la Ricerca in Agricoltura e L’analisi Dell’economia Agraria. *Italian Agriculture in Figures 2022*; CREA Consiglio per la Ricerca in Agricoltura e L’analisi Dell’economia Agraria: Roma, Italy, 2022.
88. Vasileiadou, A.; Zoras, S.; Iordanidis, A. Bioenergy Production from Olive Oil Mill Solid Wastes and Their Blends with Lignite: Thermal Characterization, Kinetics, Thermodynamic Analysis, and Several Scenarios for Sustainable Practices. *Biomass Convers. Biorefinery* **2021**, *13*, 5325–5338. [[CrossRef](#)]

89. Federacciai. *La Siderurgia Italiana in Cifre: The Italian Steel Industry Key Statistics 2022*; Federacciai: Milano, Italy, 2023; Available online: https://federacciai.it/wp-content/uploads/2023/05/AssembleaAnnuale2023_Relazione-Annuale-2022.pdf (accessed on 28 July 2024).
90. Method for Direct Reduction of Iron Oxide-Based Material for The Production of Steel, Iron Sponge or Cast Iron. WIPO Patent Application WO/2024/013653, 18 January 2024.

Disclaimer/Publisher's Note: The statements, opinions and data contained in all publications are solely those of the individual author(s) and contributor(s) and not of MDPI and/or the editor(s). MDPI and/or the editor(s) disclaim responsibility for any injury to people or property resulting from any ideas, methods, instructions or products referred to in the content.